Progress in the development of a high power helicon plasma source for the Materials Plasma Exposure Experiment

R. H. Goulding[1], J. B. O. Caughman[1], J. Rapp[1], T. M. Biewer[1], T. S. Bigelow[1], I. H. Campbell[1], J. F. Caneses[1], D. Donovan[1], N. Kafle[2], E. H. Martin[1], H. B. Ray[2], G. C. Shaw[2], M. A. Showers[2]

[1]*Oak Ridge National Laboratory, Oak Ridge, TN 37831, USA*

[2]*University of Tennessee, Bredesen Center, Knoxville, TN 37996, USA*

Contact:

R. H. Goulding
Oak Ridge National Laboratory
P.O. Box 2008 MS 6169
Oak Ridge, TN 37831-6169 USA
gouldingrh@ornl.gov

Abstract # 18387

5 pages, 6 figures

Proto-MPEX is a linear plasma device being used to study a novel RF source concept for the planned Material Plasma Exposure eXperiment (MPEX), which will address plasma-materials interaction (PMI) for nuclear fusion reactors. Plasmas are produced using a large diameter helicon source operating at a frequency of 13.56 MHz at power levels up to 120 kW. In recent experiments the helicon source has produced deuterium plasmas with densities up to ~ 6×10^{19} m^{-3} measured at a location 2 m downstream from the antenna and 0.4 m from the target. Previous plasma production experiments on Proto-MPEX have generated lower density plasmas with hollow electron temperature profiles and target power deposition peaked far off axis. The latest experiments have produced flat T_e profiles with a large portion of the power deposited on the target near the axis. This and other evidence points to the excitation of a helicon mode in this case.

KEYWORDS: MPEX helicon plasma deuterium

I. Introduction

Helicon RF plasma sources have found application in the areas of semiconductor manufacturing[1], space electric propulsion[2], and more recently for plasma-materials interactions studies[3] owing to their efficient plasma production[4-7]. Helicon sources often operate with argon, but for fusion-related PMI, it is necessary to use relevant light ion species such as helium and deuterium. It is also necessary to achieve source plasma densities n_e in the mid-10^{19} m^{-3} range or higher in order to provide relevant source particle fluxes > 10^{23} m^{-2} s^{-1} [8]. A magnetic field strength $|B|$ > 1T is desirable in some regions of the device to allow efficient additional RF ion and electron heating to be applied for the purpose of achieving a wide range of divertor-relevant parameters at the target, and a comparable value of $|B|$ at the target itself is useful for the attainment of divertor-relevant erosion product transport there. The magnetic field near the helicon antenna itself can be significantly lower, in order to achieve the highest possible n_e value. In this paper, we report on experiments with deuterium helicon plasmas in the Prototype Materials Plasma Exposure eXperiment (Proto-MPEX) linear PMI device in which this density level has been achieved, and suggest a path forward to achieve further performance improvements.

Past helicon experiments utilizing hydrogen and deuterium have typically operated at densities of several times 10^{18} m^{-3} or less[9-12]. However, experiments on the "Mini-RFTF" device at the Oak Ridge National Laboratory showed that the presence of a downstream magnetic field peak could increase the density of a light ion (He, H, D) helicon plasma by an order of magnitude[13-16]. Since then, other devices with similar magnetic field configurations have also produced high hydrogen and/or deuterium densities[3,17-20]. The Proto-MPEX helicon source uses this scheme as well, with the addition of an upstream mirror peak.

Many experiments using heavy ions have achieved high density operation only in the regime $\omega > \omega_{LH}$[21-23], where ω_{LH} is the lower hybrid frequency. Efficient heating in these experiments is associated with damping of Trivelpiece-Gould (TG) modes, with increased core heating occurring when a significant radial density gradient is present[24]. These short wavelength electrostatic waves are readily damped by collisions with ions and neutrals.

In contrast, light ion helicon operation often occurs in the regime with $\omega < \omega_{LH}$, in which case TG modes are confined radially to a thin layer at the plasma edge, where $n_e < 10^{17}$ m^{-3} for our experimental conditions. Past experiments have shown however that power can still be coupled efficiently in this regime provided that helicon "radial eigenmodes" are excited; in other words, the frequency, magnetic field, and plasma density correspond to values at which an integer number of half-wavelengths of the helicon wave, which does propagate, fit within the

plasma column transverse to the axis[15-16]. These are much longer wavelength electromagnetic waves that are more weakly damped collisionally, but in this case the resonantly enhanced electric field can still produce efficient power transfer to the electrons. Based on the experimental evidence discussed below, it appears that this condition has been achieved in the experiments discussed here. The "helicon modes" thus excited have resulted in measured D plasma densities up to ~ 6×10^{19} m^{-3}, observed ~2 m axially from the antenna, in the presence of a maximum device magnetic field $|B|$=1.3 T. We believe that this is the highest plasma density achieved to date for a helicon source operating with deuterium.

II. Experimental Description

Figure 1 shows a cutaway view of the Proto-MPEX device together with a profile of $|B|$ on axis. At the left end is a stainless steel dump plate that intercepts plasma flowing upstream from the helicon region. Magnetic field coils are indicated in dark gray; the first of a total of twelve is labeled. Next is the helicon plasma source itself, consisting of a 25 cm long, 15 cm diameter helicon antenna located in air, surrounding a cylindrical aluminum nitride vacuum window with the inner surface located at a radius of 6.3 cm. The antenna operates at 13.56 MHz at input power levels up to 120 kW. There is a gas injection region located 20 cm "downstream" from the antenna, where gas is injected at 8 azimuthal locations spaced equally around the vacuum vessel.

A thin stainless steel limiter plate with a central hole 5.8 cm in diameter separates the helicon source region from the central chamber (blue) in which 4 kW of electron cyclotron heating (ECH) at 18 GHz is applied for pre-ionizing the gas. Experiments have also begun introducing electron-Bernstein wave electron heating at 28 GHz in this region, eventually at power levels up to 200 kW, which are not discussed here. There is a double Langmuir probe (DLP), labeled "PROBE A" in the figure, located at the minimum-B point in this chamber that can be scanned vertically through the plasma column.

Beyond the central chamber is an aluminum limiter and fused quartz sleeve with an 8.6 cm inner diameter. The sleeve is 60 cm in length. There is a 25 cm long ion cyclotron antenna surrounding the sleeve that is being used for ion cyclotron heating experiments that are in the preliminary stage. Located beyond the sleeve is a second radially moveable DLP, "PROBE B" used to obtain additional n_e and T_e data, followed by a third labeled "PROBE C" in the next chamber downstream. Finally, there is a ~1.5 mm thick stainless steel target plate, the back of which is imaged

by an IR camera. It provides a 2-D measurement of the target temperature rise (ΔT) allowing power deposition on it to be estimated.

From the magnetic field profile, it can be seen that $|B|$ is low in the helicon region, ~ 0.07 T, increasing in the downstream direction to a maximum of 1.3 T in the ion cyclotron heating section. For the experiments reported here, D gas is injected at a flow rate of 2 standard liters per minute (SLM), beginning 0.3 s before application of the helicon power. At a time 50 ms before the helicon power is switched on, the gas flow is reduced to ~ 0.5 SLM, and the ECH pre-ionization power is applied. The helicon power pulse is then applied for 160 ms.

III. Results

Figure 2 shows a time profile of n_e and T_e on axis, for two pulses, obtained from "probe C" located as shown in Figure 1. For the case shown by the solid line, there is transition between two equilibrium modes, with the second having a factor of ~ 3 higher density than the first, attaining $n_e \sim 5 \times 10^{19}$ m^{-3}, with T_e dropping slightly to ~ 1.8 eV. It has been found consistently that there is a power threshold for the transition to occur, with forward power ~ 110 kW. The reflected power is typically 15% during the high-density phase, so that the threshold in net power is ~ 95 kW. The two pulses shown occurred at the power threshold, with no changes made to any of the experimental inputs. The transition is only seen to occur with gas introduced a short time before the pulse; the chamber is initially at the base vacuum pressure typically < 4mPa. It has not been observed to occur when instead the chamber is pre-filled with gas to an equilibrium pressure.

Figure 3 shows radial profiles of n_e and T_e for probe B at three different times in the pulse. Several features are noteworthy: 1) The T_e profile flattens between the early and intermediate phase, but is flattest after the transition. 2) The profile is not symmetric about the axis, and 3) The fluctuation levels in n_e and T_e, as evidenced by the size of the error bars, are significantly lower after the transition than before.

Radial n_e and T_e profiles obtained after the transition for the three probes are shown in Figure 4. The maximum density is similar in all three regions, but broader in the profile measured with probe A due to flux tube expansion there. All of the profiles show an asymmetry in n_e about the axis, although it is important to note that probes A and B were scanned vertically while C was scanned horizontally. Also, in all three regions the T_e profile is nearly flat except for a modest increase of ≤ 2 eV at the edge.

Figure 5 shows a comparison between IR images of target ΔT for a shot in which no transition occurred and one in which one did. When there is no transition (Figure 5a) the highest power deposition is observed only in a localized area at the edge of the heated region, while when there is a transition (Figure 5 b), a large fraction of the power deposition is in the central region of the target. The maximum ΔT for Figure 5b is ~ 7°C, which is roughly consistent with the rise that would be expected, assuming maximum n_e and T_e corresponding to those measured by probe C located ~ 0.4 m away that are shown in Figures 4c and 4d, using methods of comparison described in Reference 26.

Finally, Figure 6 shows the dependence of the maximum plasma density on $|B|$ at the antenna for times before and after the transitions. It can be seen that for values of $|B| < 0.065$ T, there is a linear dependence of n_e on $|B|$ for the times after the transition, while there is no such dependence evident for the times before it.

IV. Discussion

The results shown here are an indication that the jump to high density involves excitation of a helicon mode, resulting in production of a high density D plasma that propagates to the target. During the initial plasma buildup, the bulk of the heating occurs at the edge of the plasma, as evidenced by the high T_e there (Figure 3) and the edge dominated power deposition profile on the target (Figure 5). This heating may be due to TG modes confined to the edge plasma, or to near-field capacitive or inductive coupling. After the transition, the sharp rise in central density simultaneous to the flattening of the T_e profile, and the increased ΔT near the center of the target suggest that the power deposition on average moves closer to the axis, consistent with the excitation of a helicon mode. The azimuthally asymmetric edge pattern is qualitatively similar to visible light images found in References 27 and 28, obtained for low power helicon discharges, although in the latter, the asymmetry is attributed to a Faraday shield gap.

The transition from edge heating by TG modes to core heating by the helicon wave as the plasma density is increased in a helicon source has also been observed in numerical models[29]. We have begun similar modeling on our device.

In addition to the core power deposition becoming large, another indication of helicon mode excitation is the observed dependence of density on $|B|$ in the helicon region. The expected behavior can be found by examining the

$$J_1(Ta) = 0 \quad (1)$$

simplified case of a radially uniform cylindrically bounded plasma that is infinite in the axial direction. In that case the radial boundary condition satisfies the equation[30]

where J_1 is the first order Bessel function of the first kind, T is the radial wavenumber, and a is the plasma radius.

The plasma density is related to this radial wavenumber, which is thus fixed for a particular mode number and plasma radius, through the dispersion relation:

$$n_e = T\frac{k_z\ B}{\omega e \mu_0} \quad (2)$$

where k_z is the parallel wavenumber. The most efficient wave coupling occurs when the value of k_z determined from the dispersion relation matches the peak in the antenna RF vacuum spectrum which depends on antenna geometry. For T and k_z thus fixed, from Equation 2 it is expected that the plasma density for which power is most efficiently coupled increases linearly with $|B|$, and such dependence is further evidence of excitation of a helicon mode.

This behavior has been previously observed in a smaller diameter high density helicon source operating in the regime $\omega < \omega_{LH}$[15]. The flattening of the density increase, and later decrease above a certain $|B|$ value is believed due chiefly to the finite power available to produce higher density. An analysis of the stability of helicon modes that helps to further explain such behavior can be found in one of the references[25]. It is applied there to power coupling to electrons from TG modes, but the same reasoning is valid for coupling from helicon waves. The curve shown in Figure 6 obtained before the mode jump does not exhibit this behavior, suggesting that a helicon mode has not been established at that time.

The linear increase of n_e with $|B|$ can likely be extended to higher $|B|$ values if the available power is increased. In addition, increased $|B|$ in the helicon plasma production region maps to a broader plasma profile at the target. Our vacuum window has been designed to handle higher power than the available 120 kW, and the antenna has shown no sign of a power limit at this power, so that following this scaling, increasing the power further could provide significant further improvements in performance.

V. Conclusions

Experiments have been performed whose results indicate that a helicon mode with dominant core heating has been produced in Proto-MPEX, producing plasma densities in the 6×10^{19} m^{-3} range at a distance 2 m downstream of the antenna and 0.4 m from the target. Based on the dispersion relation for a helicon wave having a cylindrical boundary, it should be possible to operate at higher helicon $|B|$ with additional heating power. This can be expected to produce broader plasma profiles in high field regions, as well as possible further density increases.

This material is based upon work supported by the U.S. Department of Energy, Office of Science, Office of Fusion Energy Sciences, under contract number DEAC05-00OR22725.

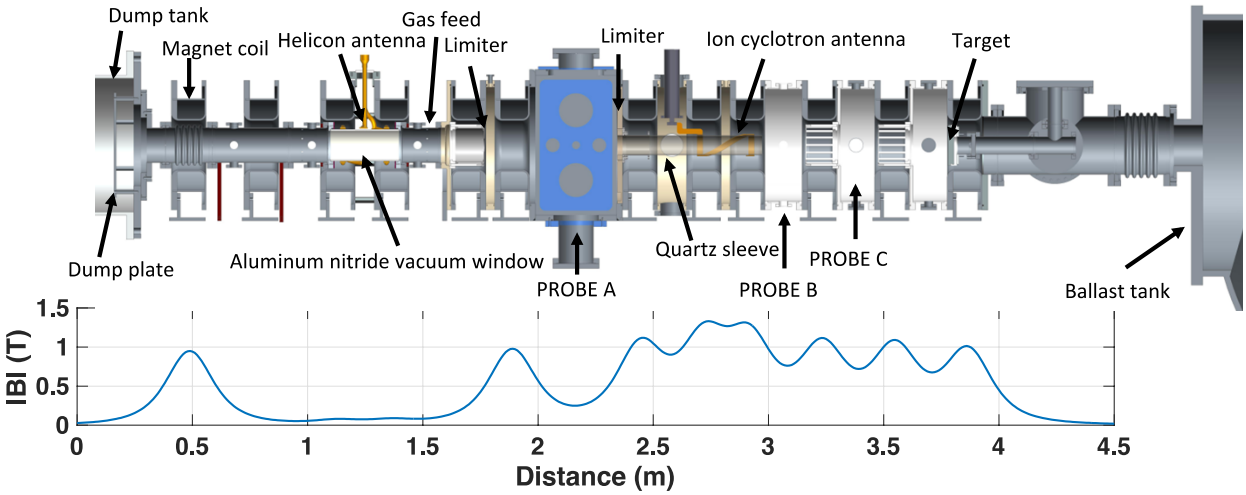

Figure 1. Proto-MPEX and magnetic field strength on axis.

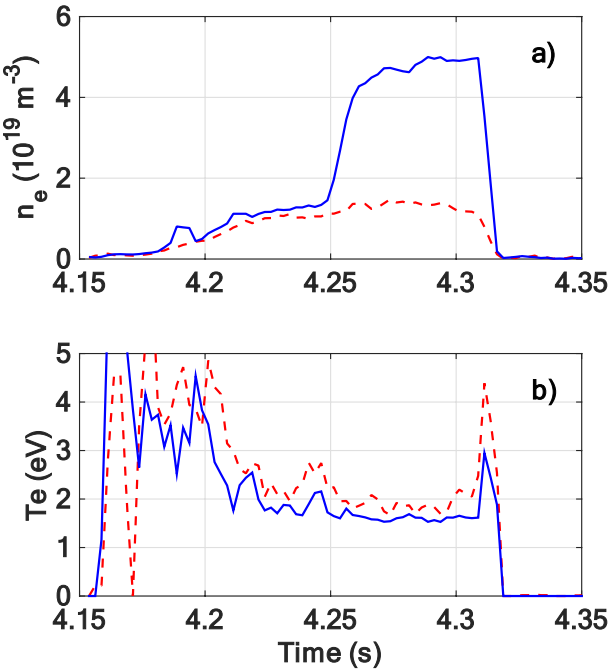

Figure 2. a) plasma density, and b) electron temperature for two shots with (solid line) and without (dashed line) mode transitions measured on axis with double Langmuir probes (Probe B).

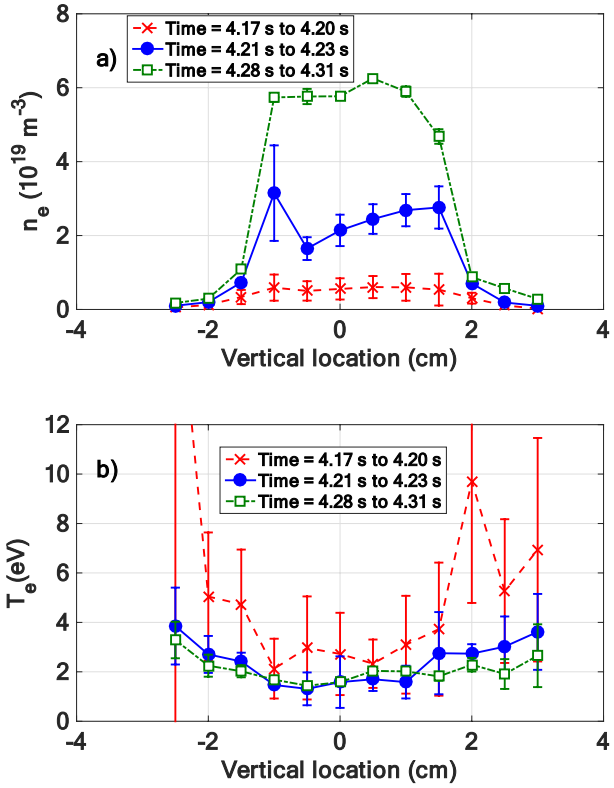

Figure 3. Radial profiles of a) n_e and b) T_e before and after the mode transition occurs, obtained with Probe B.

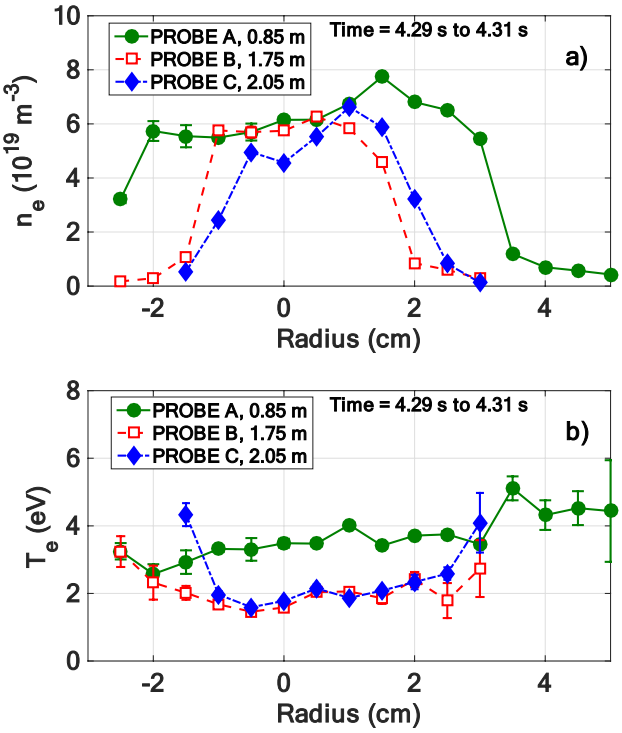

Figure 4. Radial profiles of a) n_e and b)T_e obtained using probes A (circles, solid line), B (squares, dashed line), and C (diamonds, dash-dotted line). The distances shown in the legend are distances between the helicon antenna and probe.

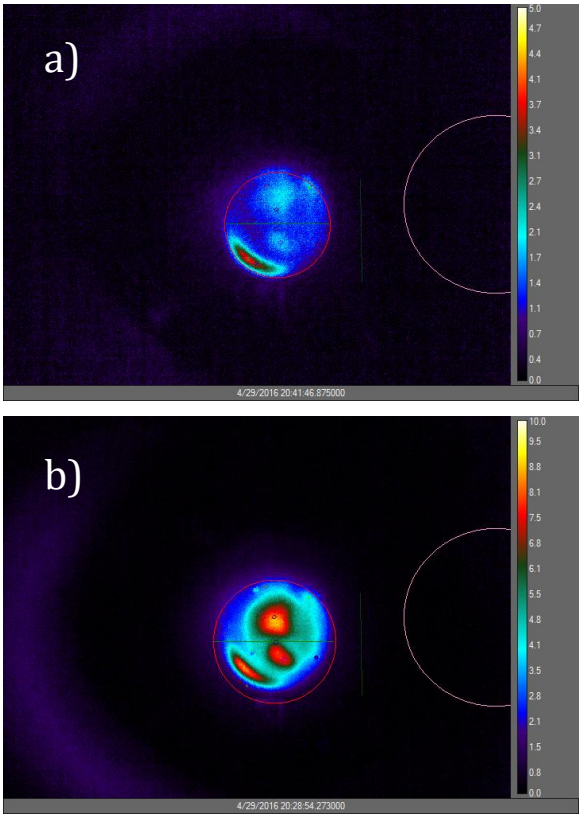

Figure 5. a) IR view of rear of target after plasma shot with no mode transition, and b) IR view after shot with a mode transition. Scale on both plots are in ^{o}C.

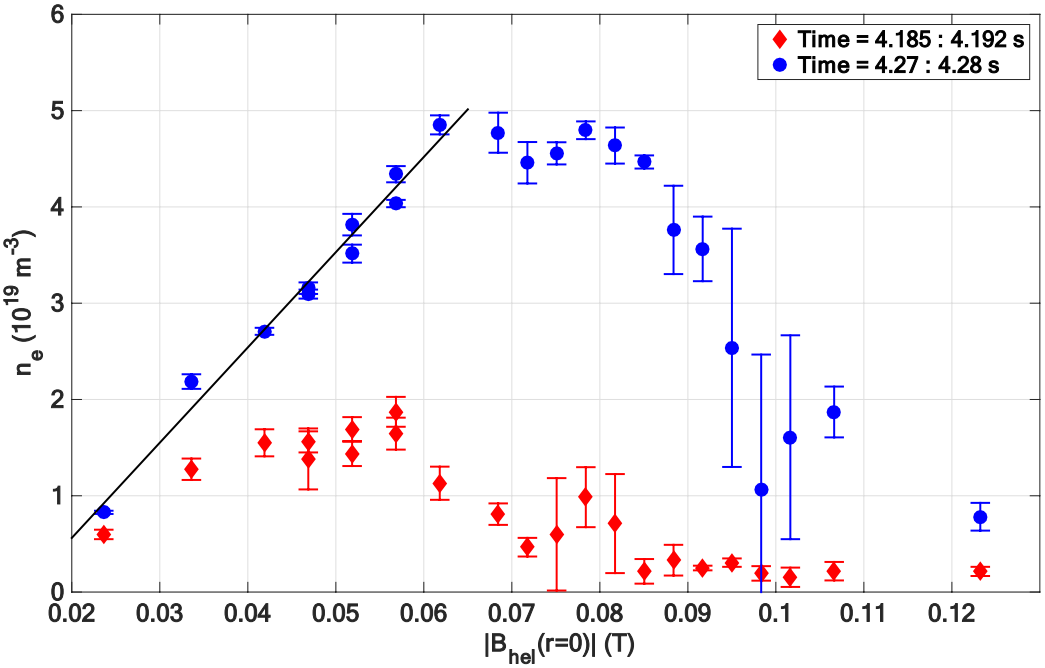

Figure 6. Plasma density vs. magnetic field strength at the helicon antenna for Probe B measured on axis for times before (diamonds), and after (circles) the high density mode transition. The solid line is a linear fit for field values up to 0.06 T after the transition.

[1]A. J. PERRY et al., "The application of the helicon source to plasma processing," *Journal of Vacuum Science and Technology B*, **9**, 310 (1991).

[2]F. R. CHANG DIAZ, "The VASIMR rocket," *Scientific American*, **283**, 90 (2000).

[3]B. D. BLACKWELL et al., "Design and characterization of the Magnetized Plasma Interaction Experiment (MAGPIE) : A new source for plasma-material interactions studies," *Plasma Sources Science and Technology*, **21**, 055033 (2012).

[4]R. W. BOSWELL, "Very efficient plasma generation by whistler waves near the lower hybrid frequency", *Plasma Physics and Controlled Fusion*, **26**, 1147 (1984).

[5]R. W. BOSWELL and F. F. CHEN, "Helicons – the early years," *IEEE Transactions on Plasma Science*, **25**, 1229 (1997).

[6]F. F. CHEN and R. W. BOSWELL, "Helicons – the past decade," *IEEE Transactions on Plasma Science*, **25**,1245 (1997).

[7]F. F. CHEN, "Helicon discharges and sources: a review," *Plasma Sources Science and Technology*, **24,** 014001 (2015).

[8]J. Rapp et al., "Transport simulations of linear plasma generators with the B2.5-Eirene and EMC3-Eirene codes," *Journal of Nuclear Materials,* **390-391**, 510 (2015).

[9]M. LIGHT et al., "Quiescent and unstable regimes of a helicon plasma," *Plasma Sources Science and Technology*, **11**, 273 (2002).

[10]Y. SAKAWA, et al., "Production of high density hydrogen plasmas by helicon waves in a simple torus," *Physics of Plasmas*, **11**, 311 (2004).

[11]T. ZIEMBA et al., "High power helicon propulsion experiments," Space Technology and Applications International Forum, Albuquerque, New Mexico, February 13-17, 2005, *AIP Conf. Proc,* **746**, 965 (2005).

[12]H. YAMAGUCHI et al., "Composition of positive ions in high-density H_2 plasmas measured by time of flight mass spectrometry," *Japanese Journal of Applied Physics*, **42**, 7080 (2003).

[12]X. M. GUO, et al., "Helicon experiments and simulations in nonuniform magnetic field configurations," *Physics of Plasmas,* **6**, 3400, 1999.

[13]R. H. GOULDING et al., "Helicon plasma source configuration analysis by means of density measurements," *Proceedings of the International Conference on Electromagnetics in Advanced Applications* (ICEAA 99), Torino, Italy, September 13-17 1999, "SciTech Connect" , http://www.osti.gov/scitech/biblio/14605 ,(Current as of September 11, 2016).

[14]M. D. CARTER et al., "Comparing experiments with modeling for light ion helicon plasma sources," *Physics of Plasmas*, **9**, 5097 (2002).

[15]Y. MORI et al., " High density hydrogen helicon plasma in a non-uniform magnetic field," *Plasma Sources Science and Technology*, **13**, 424 (2004)

[16] M. YOSHITAKA et al., "Focusing magnetic field contribution for helicon plasma on Mini-RFTF," *Thin Solid Films* **506-507**, 583 (2006).

[17]J. P. SQUIRE et al., "High power light gas helicon plasma source for VASIMR," *Thin Solid Films*, **506-507**, 579 (2006).

[18]E. A. BERING III et al., "Recent improvements in ionization costs and ion cyclotron heating efficiency in the VASIMR engine," *44th American Institute of Aeronautics and Astronautics Aerospace Sciences Meeting and Exhibit*, 9-12 January 2006 (American Institute of Aeronautics and Astronautics, Reno, NV, 2006).

[19]E. A. BERING III et al., "Observations of single-pass ion cyclotron heating in a trans-sonic flowing plasma," *Physics of Plasmas*, **17**, 043509 (2010).

[20]J. F. Caneses, to be published

[21]J. G. KWAK et al., "Frequency dependence of the plasma density for helicon plasmas," *Physics of Plasmas*, **4**, 1463 (1997).

[22]S.M. YUN et al., "Frequency dependence of helicon wave plasmas near lower hybrid resonance frequency," *Journal of Vacuum Science and Technology A*, **15**, 673 (1997).

[23]S. CHO et al., “The role of the lower hybrid resonance in helicon plasmas,” *Physics of Plasmas*, **7**, 417 (2000).

[24] D. ARNUSH, “The role of Trivelpiece-Gould waves in antenna coupling to helicon waves,” *Physics of Plasmas* **7**, 3042 (2000).

[25]K. P. SHAMRAI, “Stable modes and abrupt density jumps in a helicon plasma source,” *Plasma Sources Science and Technology*, **7**, 499 (1998).

[26]M. SHOWERS et al., Conference Proceedings HTPD-RSI, to be published in *Review of Scientific Instruments*

[27]C. MA et al., “The evolution of discharge mode transition helicon plasma through ICCD images ,” *IEEE Transactions on Plasma Science*, **43**, 3702 (2015).

[28]D. D. BLACKWELL and F. F. CHEN, “Two dimensional imaging of a helicon discharge,” *Plasma Sources Science and Technology*, **6**, 569 (1997).

[29]Y. MOUZOURIS and J. E. SCHARER, “Wave propagation and absorption simulations for helicon sources,” *Physics of Plasmas* **5**, 4253 (1998).

[30]F. F. CHEN, “Physics of helicon discharges,” *Physics of Plasmas* **3**, 1783 (1996).